OPEN ACCESS
IOP Publishing | Songshan Lake Materials Laboratory
MATERIALS FUTURES
Mater. Futures 4 (2025) 045102 (12pp)
https://doi.org/10.1088/2752-5724/adfd76

CuCl/Ph_3P-catalyzed multicomponent polymerization of CO_2 to prepare functional poly(alkynoate)s and fused heterocyclic polymers under atmospheric pressure and near ambient temperature

Tingzhu Duan[1,2], Tianbai Xiong[1,2], Lei Li[2], Jia Wang[2,*] and Xin Wang[2,*]

[1] School of Environment and Civil Engineering, Dongguan University of Technology, Dongguan 523808, People's Republic of China
[2] Songshan Lake Materials Laboratory, Dongguan 523808, People's Republic of China

E-mail: wangjia@sslab.org.cn and wangxin@sslab.org.cn

Received 19 May 2025, revised 27 July 2025
Accepted for publication 20 August 2025
Published 16 September 2025

Abstract

The conversion of CO_2 into polymeric materials is a straightforward strategy for stable long-term carbon fixation and possible carbon revitalization if introduced with functionality. Yet, such conversion has long been compromised by expensive catalysts and harsh conditions due to the inactivity of CO_2. In this work, we establish an efficient CuCl/Ph_3P-catalyzed multicomponent polymerization of CO_2, diynes, and dihalides under mild conditions of rt—60 °C and atmospheric pressure. The polymerization shows great monomer universality, producing diverse poly(alkynoate)s in yields up to 99% with weight-average molecular weights up to 94 000. Poly(alkynoate)s containing tetraphenylethylene (TPE) moieties show typical aggregation-induced emission features, and can specifically and sensitively detect Fe^{3+} ions with a low limit of detection (LOD) of 1.79×10^{-7} M. Notably, owing to lots of activated triple bonds in the main chain of poly(alkynoate)s, N-hydroxyphthalimide derivatives are facilely introduced into this polymerization *in situ* to establish a 'one-pot, two-step, four-component' tandem polymerization to produce poly(3a-hydroxyisoxazolo[3,2-a]isoindol-8(3aH)-ones)s (PHIIOs) with 100% grafting ratio. Interestingly, the fused heterocyclic PHIIO containing TPE could realize the specific and sensitive detection of Ag^+ ions with a low LOD of 4.90×10^{-6} M. This work not only innovatively achieves the direct chemical fixation of CO_2 into functional polymeric materials under relatively low temperatures with low-cost catalysts, but also obtains a series of polymers with controllable structure-function, which can be realized for a wide range of applications.

* Authors to whom any correspondence should be addressed.

Supplementary material for this article is available online

Keywords: CO_2, atmospheric pressure, room temperature, multicomponent polymerization, fused heterocyclic polymers

1. Introduction

Carbon dioxide (CO_2) is an important raw material for the photosynthesis of green plants. However, since the Industrial Revolution, the extensive use of fossil fuels has resulted in a large amount of CO_2 being emitted [1]. As a greenhouse gas, the continuous rise of CO_2 in the atmosphere will cause serious environmental and climate problems, such as melting glaciers, rising sea levels, abnormal climate, and desertification [2]. Therefore, it is of great significance to achieve the conversion of CO_2 while reducing its emissions.

Polymer functionalization of CO_2 is a strategy that kills two birds with one stone. On the one hand, CO_2 is consumed; on the other hand, CO_2 can be converted into high value-added functional polymeric materials, which always show good degradability including ester or carbonic ester units [3]. However, CO_2 is a nonpolar molecule, with the highest oxidation state of carbon. As a result, it exhibits excellent thermodynamic stability [4]. To achieve the conversion of CO_2, highly active catalysts and high-energy comonomers are needed to generate target products in relatively low-energy states. Except these, high reaction pressure and temperature are necessary, especially for industry-scale production [5–8]. High pressure is potentially dangerous and has caused many production accidents, while high temperatures will lead to high energy consumption, further increasing CO_2 emissions. Therefore, the development of CO_2-based polymerization at atmospheric pressure with lower conversion temperature is significant.

Recently, multicomponent polymerizations (MCPs) stand out for the co-introduction of several active monomers [9–25], which are conducive to the fixation of CO_2 at mild condition, especially triple-bond monomers based MCPs for their rich reaction types and high activity. For example, Qin's group established a $PdCl_2$/PPh_3/DBU-catalyzed MCP of CO_2, isocyanides, and 2-iodoanilines at 80 °C under atmosphere pressure to prepare functional poly(benzoyleneurea)s with acceptable weight-average molecular weights (M_w) (up to 8700) and satisfactory yields (up to 86%) [26]. Dong's group used a very active monomer dialkylacetylenedicarboxylate to realize a catalyst-free MCP with diisocyanate and CO_2 at 80 °C under atmospheric pressure, and spiropolymers were generated with good yields (up to 87.7%) with high M_w, (up to 59,000) [27]. Qin's group also developed a $Pd(OAc)_2$/LiO^tBu-catalyzed MCP of CO_2, internal alkyne dipropanol, and aryl dihalides at 80 °C under atmospheric pressure, and a series of linear and hyperbranched multifunctional five-membered cyclic carbonate (5CC)-based polymers were produced in high yields (up to 96%) with high M_w (up to 42,500) [28]. In addition to isocyanides and endynes, active aryl terminal alkynes can also be used to realize the MCP of CO_2 at atmospheric pressure. Oi and colleagues firstly achieved this MCP of CO_2, aromatic diyne, and alkyl dihalides at 80 °C under atmospheric pressure with CuI (scheme 1(a)), but most of the resulting polymers showed wide dispersibility indices of up to 5.66 [29]. When expanding from aromatic diyne to alkyl diyne or dibromoalkane to diiodoalkane, the yields of polymerization were lower (about 9%–34%), showing poor monomer universality. Later, Qin's group adopted a highly efficient catalyst system Ag_2WO_4 to realize this MCP to prepare poly(alkynoate)s at 80 °C under atmospheric pressure with relatively small PDI (scheme 1(b)). Whereas, this polymerization was also not suitable for diiodoalkane monomer with low molecular weight (M_w = 4600) and yield of 39% and alkyl diynes [30]. Due to the high reactivity of poly(alkynoate)s, they combined this MCP with amines to develop a four-component tandem polymerization (FCTP), and a batch of linear and hyperbranched poly(aminoacrylate)s with regio- and stereoregular structure were prepared, which were realized in the fields of drug release, fluorescent materials, precise degradation, fluorescent probes, etc [31].

The alkyne-rich backbone of poly(alkynoate)s provides versatile post-polymerization modification opportunities *in situ*, enabling precise synthesis of functional polymers with tailored properties. In this study, we addressed the challenge of monomer universality by developing a mild MCP strategy for synthesizing poly(alkynoate)s from CO_2, diynes, and alkyl dihalides. This process operates efficiently at atmospheric pressure and moderate temperatures (room temperature to 60 °C), utilizing an economical CuCl/PPh_3 catalytic system (scheme 1(c)), which was inspired by an organic reaction from He's group [32]. Not only dihalides monomers with different halogen elements (Cl, Br, I), but also aryl diyne and alkyl diyne could proceed smoothly in this MCP. A series of poly(alkynoate)s with high weight average molecular weights (M_w up to 94,000) were obtained in excellent yields (up to 99%). Notably, this polymerization also allows for gram-scale output. By successfully introducing tetraphenylethylene (TPE) groups into the main chain, the poly(alkynoate) possesses aggregation-induced emission (AIE) properties and exhibits specific fluorescence quenching for Fe^{3+} ions. In addition, this MCP could be facilely extended to a 'one-pot, two-step, four-component' tandem polymerization with N-hydroxyphthalimide (NHPI) derivatives, affording fused heterocyclic poly(3a-hydroxyisoxazolo[3,2-a]isoindol-8(3aH)-ones)s (PHIIOs). Surprisingly, PHIIO with AIE feature exhibits specific delayed fluorescence quenching for Ag^+ ions.

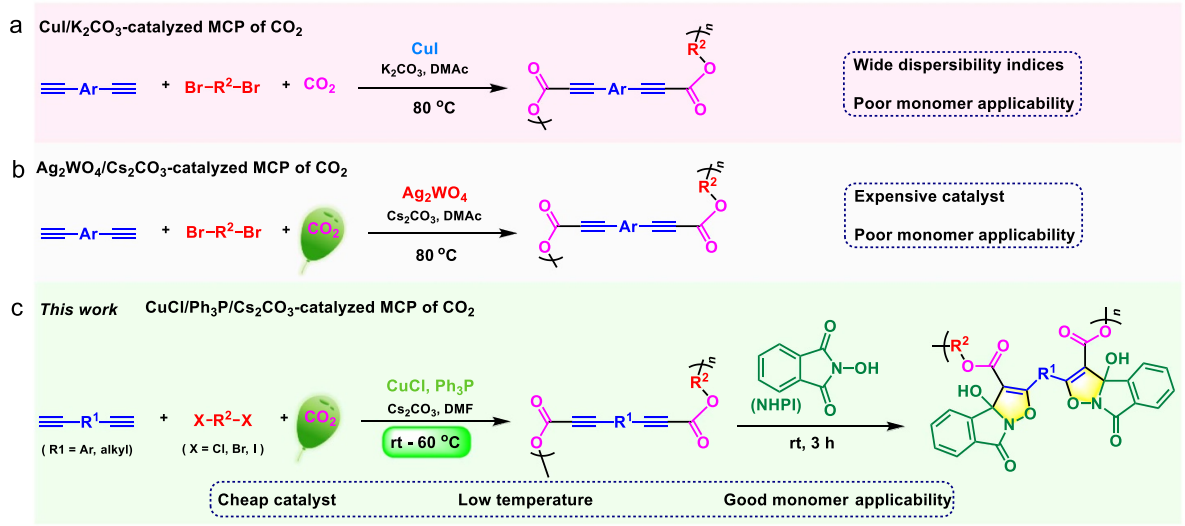

Scheme 1. The developed polymerization of terminal alkyne, dihalide, and CO_2 under atmospheric pressure.

2. Results and discussion

2.1. CuCl/PPh3-catalyzed MCP of CO2, diynes, and alkyl dihalides

Terminal alkynes **1a**—**1g** (schemes 2(S1–S7)) were first synthesized according to the reported method [33], while alkyl dihalides **2a**—**2f** were commercially available. In order to test the feasibility of this polymerization, 1,2-bis(4-ethynylphenyl)-1,2-diphenylethylene (**1a**, 0.2 M), 1,6-dibromohexane (**2a**, 0.2 M) were chosen as model monomers with a CO_2 balloon, then reacted in a Schlenk tube with N,N-dimethylformamide (DMF, 1 ml) as solvent in the presence of cheap catalyst CuCl (0.04 M), Ph_3P (0.04 M), Cs_2CO_3 (0.8 M) at 80 °C for 24 h. Later, the polymers with a low M_w of 4600 were obtained in a yield of 49%, as shown in (table S1).

Because Cs_2CO_3 as a base can not only fix as much CO_2 as possible into the reaction system, but also promote the deprotonation of terminal alkynes, so the loading of Cs_2CO_3 was firstly studied [29, 30, 32]. By gradually increasing the Cs_2CO_3 loading from 4 to 7 equivalences, the yields and M_ws were obviously improved from 49% to 99%, and 4600 to 25 100, respectively (table S1). So, 7 equivalences of Cs_2CO_3 were selected as the optimized loading for further optimization.

The monomer concentrations were then monitored, as shown in (table S2). Increasing the monomer concentration from 0.1 to 0.2 M improved the yield from 85% to 99%, and dramatically increased the M_w from 8400 to 25 100. As the monomer concentration was further increased to 0.4 M, the M_w of the polymer continued to increase, but the number average molecular weight (M_n) increased inconspicuously and the PDI increased significantly. Hence, 0.2 M of monomer concentration was taken for the next study.

After polymerization in four polar aprotic solvents separately: DMF, N-methyl-2-pyrrolidone (NMP), dimethyl sulfoxide (DMSO), and N, N-dimethylacetamide (DMAc), DMF stood out for the best polymerization results (table S3). As the

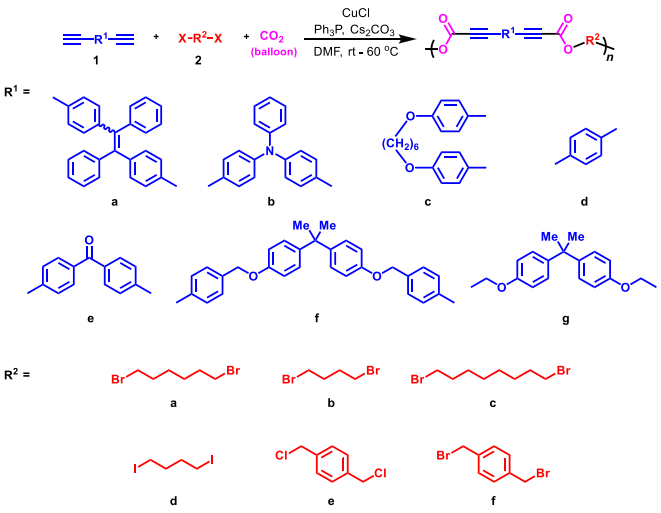

Scheme 2. MCP of terminal alkynes, dihalides, and CO_2 in the presence of $CuCl/Ph_3P/Cs_2CO_3$.

reaction time increased from 12 to 24 h, the yield and molecular weight of the polymer increased significantly (table S4). So, 24 h was the optimized reaction time. To reduce energy consumption, the reaction temperature was gradually lowered from 80 °C, and good polymerization results with a high M_w of 19 600 in 99% were obtained, even at 60 °C. The M_n (10 500) obtained for polymers is higher than that (9800) at 80 °C (table S5). So, we chose a milder, more economical and environmentally desirable condition, 60 °C as the optimized polymerization condition.

Later, different bases were used in this polymerization reaction (table S6). It is evident that Cs_2CO_3 delivered the best performance, which can be attributed to three key factors: Firstly, highly polar bases NaOH and KOH have poor solubility in DMF, while carbonate salts exhibit significantly higher solubility in DMF, which can be observed in our experiments. The radius of Cs^+ is larger than that of K^+, and its

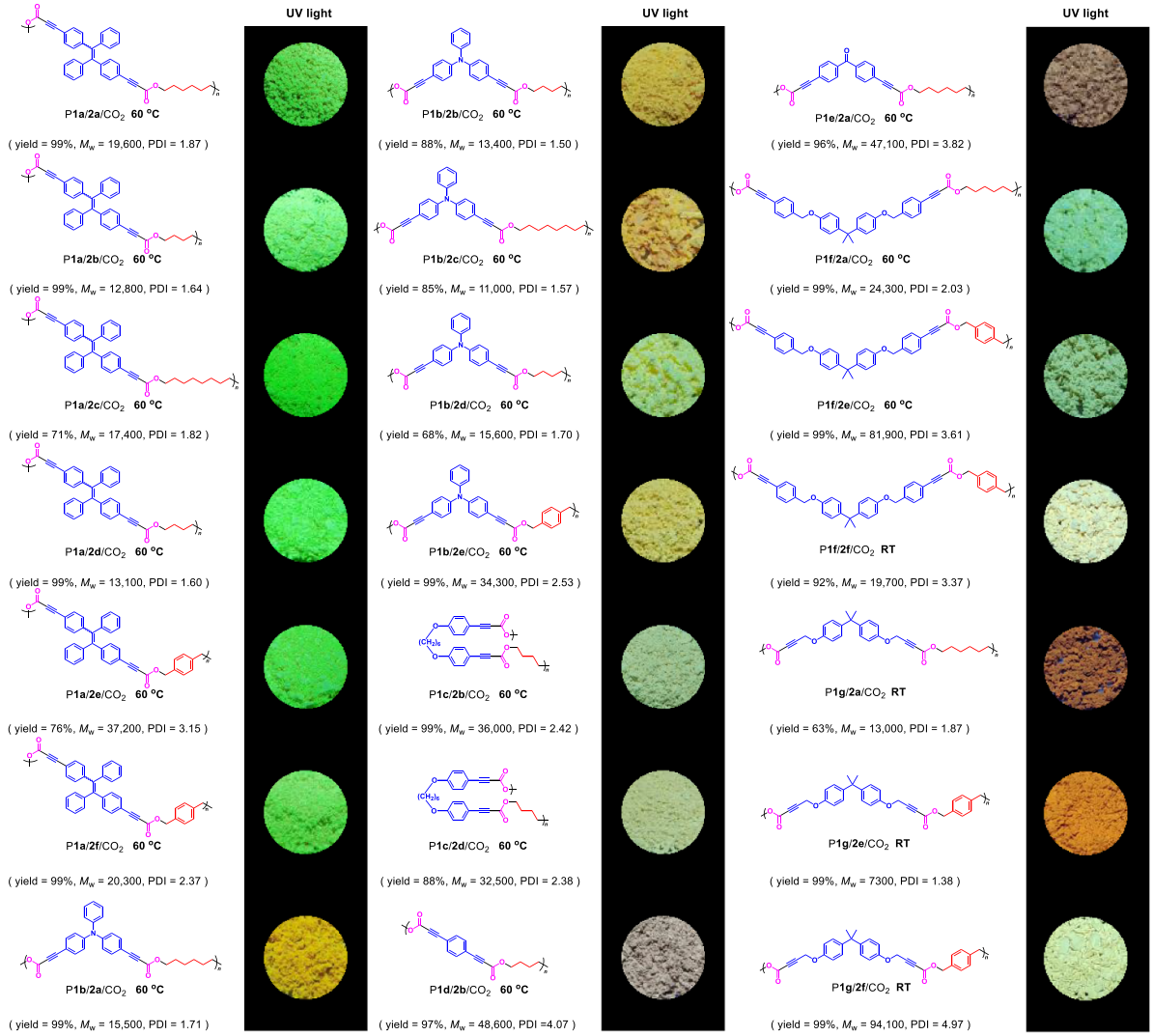

Figure 1. Polymerization results of different monomers and their corresponding solid-state fluorescence images under a 365 nm UV lamp.

solvation energy of Cs_2CO_3 is lower, further enhancing its solubility in DMF. Secondly, in terms of basicity, Cs_2CO_3 is markedly stronger than K_2CO_3. This enables efficient deprotonation of terminal alkynes to generate the key intermediate copper acetylide (R−C≡C−Cu). Thirdly, Cs_2CO_3 forms a high concentration of free CO_3^{2-} ions in DMF, which activate CO_2 via an equilibrium reaction, thereby promoting the polymerization process.

With optimized polymerization conditions in hand, diynes and dihalides (scheme 2) with different structures were conducted to check the universality and generality of this MCP (scheme 2, figure 1, and table S7). Such as, aromatic diynes with rigid conjugated structures (**1a, 1b, 1d, 1e**) or flexible nonconjugated structures (**1c, 1f**), and aromatic diynes containing electron donating (**1b, 1c, 1f**) or electron-withdrawing (**1e**) groups in the para-position of the benzene ring, polymerize well with dihalides and CO_2. In addition, aliphatic dihalides with different chain lengths (such as 1, 6-dibromohexane (**2a**), 1, 4-dibromobutane (**2b**), and 1, 8-dibromooctane (**2c**)), as well as dihalides with different halogen elements (Br, I, Cl) were utilized in this MCP. The results showed that all polymerizations worked very well and polymers with high M_w values (up to 81,900) and excellent yields (up to 99%) were obtained, indicating that the polymerization has universal applicability to various monomers. Active benzyl halides (**2e, 2f**) had better polymerization with diynes and CO_2 than alkyl halides. Notably, the more reactive 1,4-bis(bromomethyl)benzene (**2f**) could be combined with alkyl alkyne (**1g**) and CO_2 to give poly(alkynoate) in 99% yield with high M_w of 94 000 at room temperature under atmospheric pressure. The high activity of **1g** primarily stems from its propargyl ether structure (C≡C−CH_2O−). Compared to aryl-substituted alkynes, this structure exhibits greater nucleophilicity, and can more readily bind to the electrophilic metal center, forming a more stable or reactive metal-propargyl ether intermediate (M−C≡C−CH_2O−). This makes the activation step faster and more favorable, enabling the successful fixation and carboxylation of CO_2 under mild conditions. This is the first

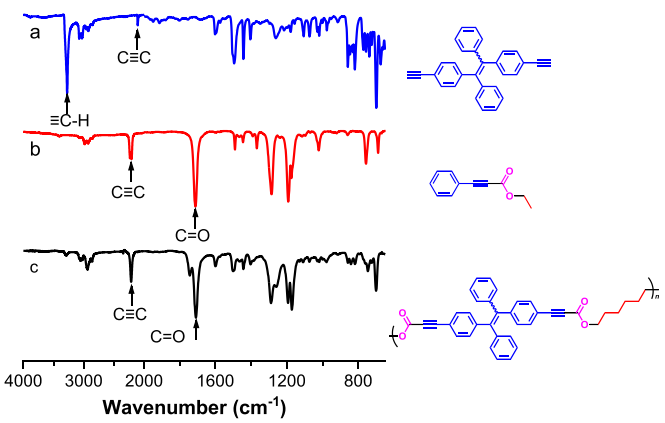

Figure 2. FT-IR spectra of (a) monomer **1a**, (b) model compound **3**, and (c) polymer P**1a/2a**/CO_2.

time to our knowledge that the chemical fixation and conversion of CO_2 into high molecular weight poly(alkynoate) has been achieved at room temperature and atmospheric pressure.

Furthermore, due to the high efficiency and mild reaction conditions of the MCP, a large-scale polymerization under the optimized conditions was carried out. The polymerization of **1b** (2 mmol) and **2a** (2 mmol) in 10-fold doses with CO_2 were taken as an example, generating 1.01 g of P**1b/2a**/CO_2 in 91% yield with a higher M_w of 17 900 than that of the 0.2 mmol monomer (figure S1), implying that the poly(alkynoate) has the potential to be produced on a large scale as functional polymers conveniently.

2.2. Structural characterization

To precisely verify the structure of the resulting polymers, FT-IR, ^{1}H NMR, and ^{13}C NMR were performed on all the polymers, their corresponding monomers, and commercially available model compound **3** (figures 2, 3 and S2–S61). Due to the similarity in the structure of the resulting polymers, we took P**1a/2a**/CO_2 as an example. As shown in figure 2, the stretching vibration peaks of ≡C−H and C≡C in the FT-IR spectrum of monomer **1a** are at 3293 and 2101 cm^{-1}, respectively. However, in the spectra of model compound **3** and polymer P**1a/2a**/CO_2, the stretching vibration peaks of ≡C−H disappear, and the stretching vibration peak of C≡C is shifted to 2218 cm^{-1}. The characteristic peaks at 1706 cm^{-1} in the spectra of **3** and P**1a/2a**/CO_2 are identified as the stretching vibration peak of C=O of newly formed ester groups. The results preliminarily prove that the CuCl/PPh_3-catalyzed MCP of CO_2, diynes, and alkyl dihalides is established successfully.

The structure of the obtained poly(alkynoate)s could be more accurately determined from the NMR spectra. As shown in figure 3, the alkyne protons (H^1) of monomer **1a** (figure 3(a)) and the −CH_2Br protons (H^4) of **2a** (figure 3(b)) are at δ 3.03 and 3.41, respectively, which disappear in the spectra of model compound **3** (figure 3(c)) and P**1a/2a**/CO_2 (figure 3(d)). While the methylene protons of H^2 and H^3 of **2a** resonate at 1.48, 1.88, respectively, are inherited and shift to 1.44 (H^7), 1.72 (H^8) in the spectrum of P**1a/2a**/CO_2. Notably, the new peaks resonate at δ 4.30 (H^6) and δ 4.21 (H^9) are attributed to newly formed methylene of ester groups of model compound **3** and polymer P**1a/2a**/CO_2, respectively.

The ^{13}C NMR spectra provided further evidence of the structure of the poly(alkynoate)s. The peaks at δ 77.47 (C^1) and 83.67 (C^2) are assignable to the resonances of the triple bond carbons in the spectrum of **1a** (figure 3(e)), which are retained and obviously shift to δ 80.72 (C^8, C^{14}) and 86.05 (C^9, C^{15}) in the spectra of **3** (figure 3(g)) and P**1a/2a**/CO_2 (figure 3(h)). Meanwhile, the new carbon peaks at δ 62.08 and 154.07 in the spectrum of **3**, as well as δ 65.88 and 154.10 in the spectrum of P**1a/2a**/CO_2, are attributed to the resonances of the newly generated methylene (OCH_2−) and carbonyl (C=O) of ester groups, respectively. These results clearly confirm that the efficient MCP produces poly(alkynoate)s.

2.3. Solubility and thermal stability

Poly(alkynoate)s exhibit excellent solubility not only in high polar solvents such as DMF, DMAc, and DMSO, but also in common moderate polarity solvents such as dichloromethane (DCM), chloroform, tetrahydrofuran (THF). The thermal stability of poly(alkynoate)s was studied by thermogravimetric analysis (TGA) under nitrogen atmosphere. For polymers of the same structure from different monomers, the test results for one of them are presented in (figure S62). The results showed that the temperature of 5% weight loss (T_d) was in the range of 187 °C–340 °C under nitrogen. When the temperature increased to 600 °C, the residual carbon content of most polymers was higher than 50%, indicating that the polymers had excellent thermal stability. The glass transition temperatures (T_g) of the polymers measured by differential scanning calorimetry (DSC) range from 87 °C to 127 °C (figure S63). The T_gs could be effectively regulated by the differences in monomer structures. Such as, the T_gs of P**1a/2b**/CO_2, P**1a/2a**/CO_2, and P**1a/2c**/CO_2 gradually decrease from 112 to 87 °C, showing that the longer the alkyl chain, the lower the polymer T_g. And the poly(alkynoate)s prepared from monomers **1a** or **1b** possess higher T_gs than those from other diynes, because their main chains contain more rigid structures.

2.4. Photophysical properties

Polymers with high fluorescent efficiencies in the aggregated or solid state are ideal materials for probing, bioimaging, and information encryption. It is worth noting that all prepared poly(alkynoate)s, whether they contain fluorescent moieties, exhibit apparent solid-state fluorescence under a 365 nm UV lamp (figure 1). So, this MCP show specific polymerization-induced emission [34, 35]. It is understandable that poly(alkynoate)s with fluorescent moieties could emit fluorescence, such as TPE or TPA. While, the emission behaviors of other polymers without usual luminophore can be attributed to lots of unsaturated triple bonds and ester groups in the main chain, which could generate fluorescent clusters [36]. The photophysical properties of poly(alkynoate)s were systematically studied. The maximum absorption wavelength of poly(alkynoate)s with diverse structures in diluted DMF

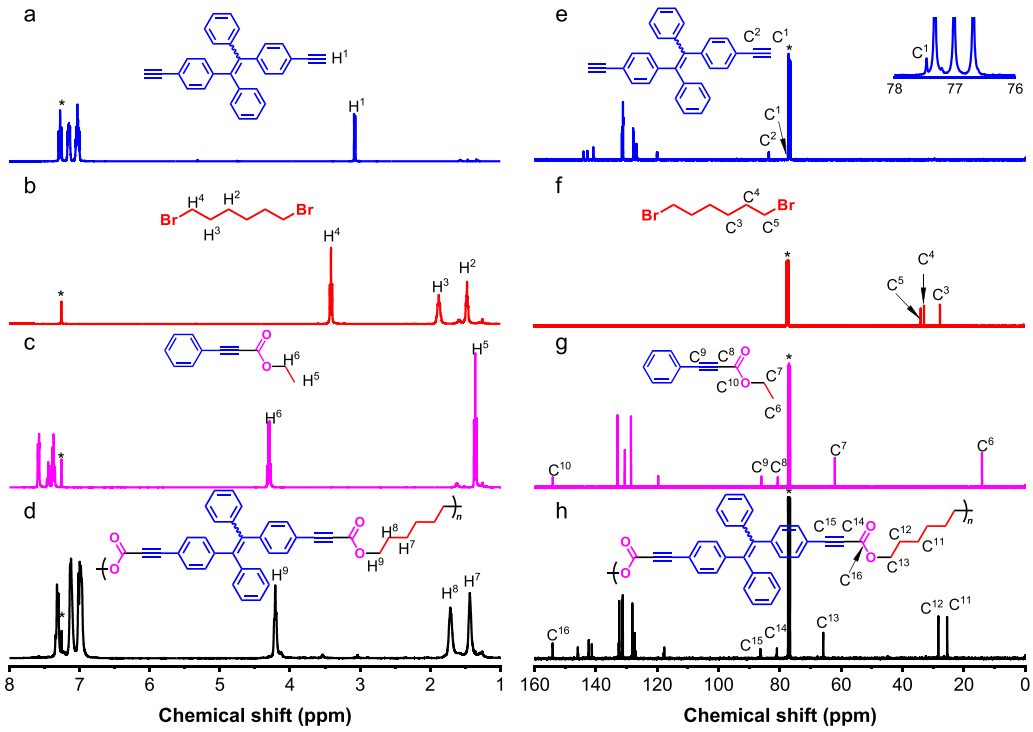

Figure 3. ^{1}H NMR spectra of (a) monomer **1a**, (b) monomer **2a**, (c) model compound **3**, and (d) polymer P**1a/2a**/CO_2, as well as corresponding ^{13}C NMR spectra of (e) **1a**, (f) **2a**, (g) **3**, and (h) polymer P**1a/2a**/CO_2 in chloroform-*d*. The solvent peaks are marked with asterisks.

solutions are in the range of 340–379 nm (figures S64(a)–(d)). Comparing the PL spectra in dilute solutions and solid powders (figures S64(e)–(l)), poly(alkynoate)s containing TPE moieties show stronger solid-state emission, whereas other poly(alkynoate)s show stronger solution-state emission. Under the excitation of the maximum absorption wavelength of 340 nm, the diluted DMF solution of P**1a/2a**/CO_2 emits a faint fluorescence with a peak at 512 nm as shown in figure 4(a). When gradually increasing the water fraction (f_w), the fluorescence gradually increases due to the aggregation behavior of the polymer chains. The fluorescence intensity of P**1a/2a**/CO_2 reaches the maximum with 70% f_w, which was 38.4 (α_{AIE}) times higher than that of their pure DMF solution (figure 4(b)). Other poly(alkynoate)s containing TPE show similar emission phenomena (figures S65–67), and the α_{AIE} values of P**1a/2b**/CO_2, P**1a/2c**/CO_2, and P**1a/2e**/CO_2 are 109.0, 74.8, and 91.2, respectively.

2.5. Fe (III) ion detection

Metal ions are important for the growth, development and normal physiological functions of living organisms. It is important to identify specific metal ions accurately and sensitively. With newly formed alkynoate groups, poly(alkynoate)s may easily complex with metal ions. So, the P**1a/2a**/CO_2 nanoaggregates with AIE feature in the DMF/water mixture with f_w of 70% were taken as an example to detect metal ions. After testing 22 cations under the same experimental conditions, namely, Fe^{3+}, Ag^{+}, Ca^{2+}, Cd^{2+}, Ce^{3+}, Co^{2+}, Cr^{3+}, Cu^{2+}, Dy^{3+}, Fe^{2+}, K^{+}, Lu^{2+}, Mg^{2+}, Na^{+}, NH_4^{+}, Ni^{2+}, Sc^{3+}, Sm^{3+}, Sr^{2+}, Y^{3+}, Yb^{6+}, and Zn^{2+}, only Fe^{3+} ions showed a significant fluorescence quenching effect (figure 4(c)). The probable quenching mechanism is that Fe^{3+} ions can stably coordinate to the alkynes [37, 38] and electron-rich groups (such as carbonyl group) [39], which causes the photoinduced electron transfer (PET) process from excited-state electrons of P**1a/2a**/CO_2 to the half-filled 3d orbits of Fe^{3+} ions, then triggering fluorescence quenching. Fe^{3+} ions may coordinate with three alkynoates to form stable six coordination structure (figures S68) [40, 41].

In addition, titration experiments proved that this AIE probe had high sensitivity to Fe^{3+} ions. Gradually adding Fe^{3+} into the nanoaggregates of P**1a/2a**/CO_2, the fluorescence intensity decreases instantly, as shown in figure 4(d). The quenching constant was calculated by the Stern–Volmer curve to be as high as 81 950 M^{-1}, and the relative PL intensity (I_0/I) showed a very good linear relationship with the concentration of Fe^{3+} ions, with a low limit of detection (LOD) of 1.79×10^{-7} M. As we all know, iron is an essential trace element for human metabolism, which is an important component of hemoglobin and a variety of enzymes [42], such as DNA synthesis and oxygen transfer in cells. Therefore, the development of Fe^{3+} fluorescent probe with environmental friendliness, simplicity, rapidity, and high sensitivity is of great significance.

2.6. FCTP

With abundant ester-activated triple bonds in the main chain, poly(alkynoate)s is hopeful to be further modified to expand their functionalities. In contrast to the post-modification of

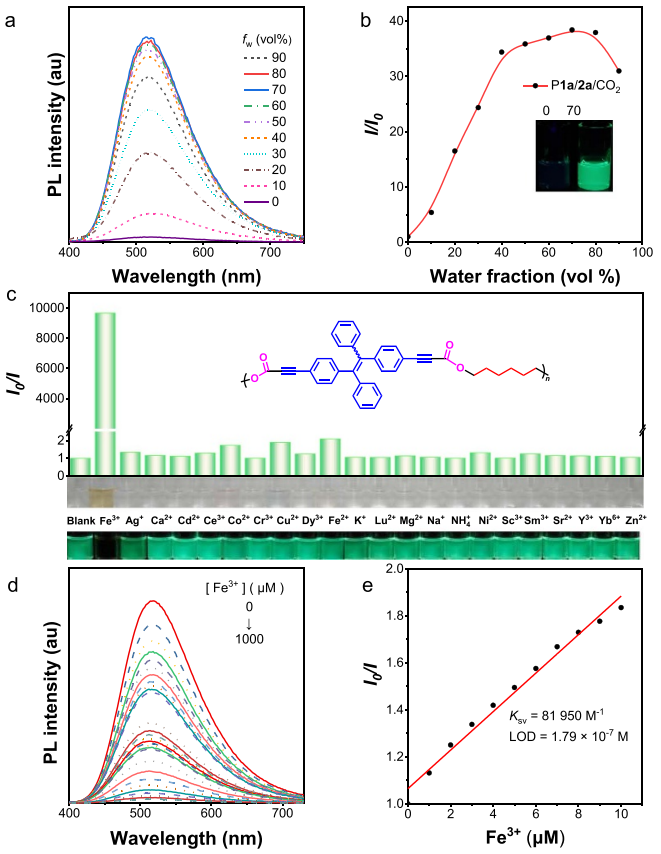

Figure 4. (a) PL spectra of P**1a/2a**/CO_2 in DMF and DMF/water mixtures. Concentration: 10 μM. λ_{ex}: 340 nm. (b) Plot of relative PL intensity versus different water fraction (f_w) in DMF/water mixtures, where I = peak intensity with different f_w and I_0 = peak intensity in DMF. Inset in panel B: fluorescence photograph of P**1a/2a**/CO_2 in DMF and a DMF/water mixture with 70% f_w. (c) Relative PL intensity (I_0/I) of P**1a/2a**/CO_2 in DMF/water mixtures (f_w: 70%) versus different metal ions, where I_0 and I are the maximal fluorescence intensity recorded before and after addition of metal ions into P**1a/2a**/CO_2 solution. Polymer concentration: 10 μM, metal ion concentration: 6 mm, λ_{ex}: 340 nm. Illustration: Photograph of polymer probe with different metal ions taken under daylight and ultraviolet light at 365 nm. (d) PL spectra of P**1a/2a**/CO_2 in response to Fe^{3+} at different concentrations. (e) The linear relationship between I_0/I and different Fe^{3+} concentrations at 512 nm, where I and I_0 are the fluorescence intensities of P**1a/2a**/CO_2 nanoaggregates with different amounts of Fe^{3+} and that without Fe^{3+}, respectively.

polymers requiring complex operations such as separation and purification, we expanded the MCP of CO_2, diynes, and alkyl dihalides into an 'one-pot, two-step, and four-component' tandem polymerization with NHPI, as shown in figure 5(a). Model compound **4** was designed and synthesized with a yield of 69%, implying the possibility of this FCTP (Scheme S8). The monomers **1b, 2a**, and CO_2 were then taken as examples to optimize the second step of this FCTP with NHPI. After systematic studying the NHPI feed ratio, reaction time, and monomer concentration (tables S8–S10), the optimum condition for the second step was that 1 ml of DMF solution of NHPI (6 equiv. to **1b**) was injected into the system to react for 3 h, and ring-fused P**1b/2a**/CO_2/NHPI with high M_w (23,500) was obtained in 76% yield. The FCTP showed good functional group tolerance, and a series of poly(3a-hydroxyisoxazolo[3,2-a] iso-indol-8(3aH)-ones)s (PHIIOs) were obtained at high yields (up to 86%) with high M_ws (up to 42 700).

The high-resolution mass spectra of model compound **4** (figure S69) and the FT-IR, NMR results of monomers, model compound **4**, and PHIIOs (figures S70–S90) further confirmed the success of this FCTP and the correctness of the PHIIO structure. As shown in (figure S70), the stretching vibration peaks of C≡C disappear in the spectra of model compound **4** and polymer P**1a/2a**/CO_2/NHPI, while the peaks of the newly formed −OH and C^2=O appear at 3402 and 1752 cm^{-1}, respectively. The results preliminarily prove that the success of the FCTP. As shown in (figure S77), the alkyne protons of monomer **1a** (figure S77(a), H^1), $BrCH_2$− of **2a** (figure S77(b), H^4), N−OH of NHPI (figure S77(c), H^5) are at δ 3.03, 3.41 and 10.81, respectively, which disappear in the spectra of model compound **4** (figure S77(d)) and P**1a/2a**/CO_2/NHPI (figure S77(e)). The methylene protons of H^2 and H^3 of **2a** resonate at δ 1.40, 1.80, respectively, are inherited and shift to 1.04 (H^7), 1.33 (H^8) in the spectrum of P**1a/2a**/CO_2/NHPI. Notably, the new peaks resonate at δ 4.30 (H^6) and δ 4.21 (H^9) are attributed to newly formed methylene of ester groups of model compound **4** and polymer P**1a/2a**/CO_2/NHPI, respectively. The triple bonds peaks at δ 76.60 (C^1) and 83.65 (C^2) (figure S77(f)) shift to 98.27 (C^{12}) and 174.15 (C^{16}) in the spectrum of P**1a/2a**/CO_2/NHPI (figure S77(j)). The peaks of $BrCH_2$− at δ 35.39 (C^3) of **2a** (figure S77(g)) shift to 64.42 (C^{11}) in the spectrum of P**1a/2a**/CO_2/NHPI, because of the newly generated methylene (OCH_2−). One of the carbonyl groups of NHPI is retained while the other is converted into C−OH. The peaks of their characteristic carbons are changed from δ 164.54 (C^4) to 162.13 (C^{14}) and 107.46 (C^{13}), respectively. At the same time, the new peak at δ 167.55 (C^{15}) is attributed to the newly formed C=O of ester groups. These results clearly confirm the successful establishment of this FCTP. The proton integral ratio of aromatic ring to −OCH_2− was 26:4 (figure S84), proving that all alkynes of poly(alkynoate)s were reacted and the grafting degrees of PHIIOs were up to 100%.

PHIIOs containing lots of O, N heteroatoms in the main chain and hydroxyl groups in the side chain, can be well dissolved in large polar solvents (DMF, DMSO, DMAc), but not soluble in relatively small polar solvents, such as THF, DCM, and $CHCl_3$. TGA and DSC results revealed PHIIOs have high thermal and morphological stabilities. The T_ds of PHIIOs are in the range of 216 °C–284 °C, which are lower than that of their corresponding poly(alkynoate)s, due to the abundance of nitrogen and oxygen atoms and hydroxyl groups in the polymer chain (figure S91). While the T_gs PHIIOs are in the range of 101 °C–148 °C, which are higher than that of their corresponding poly(alkynoate)s, due to strong hydrogen bonding interactions between hydroxyl groups and rigid fused-ring structures (figure S92).

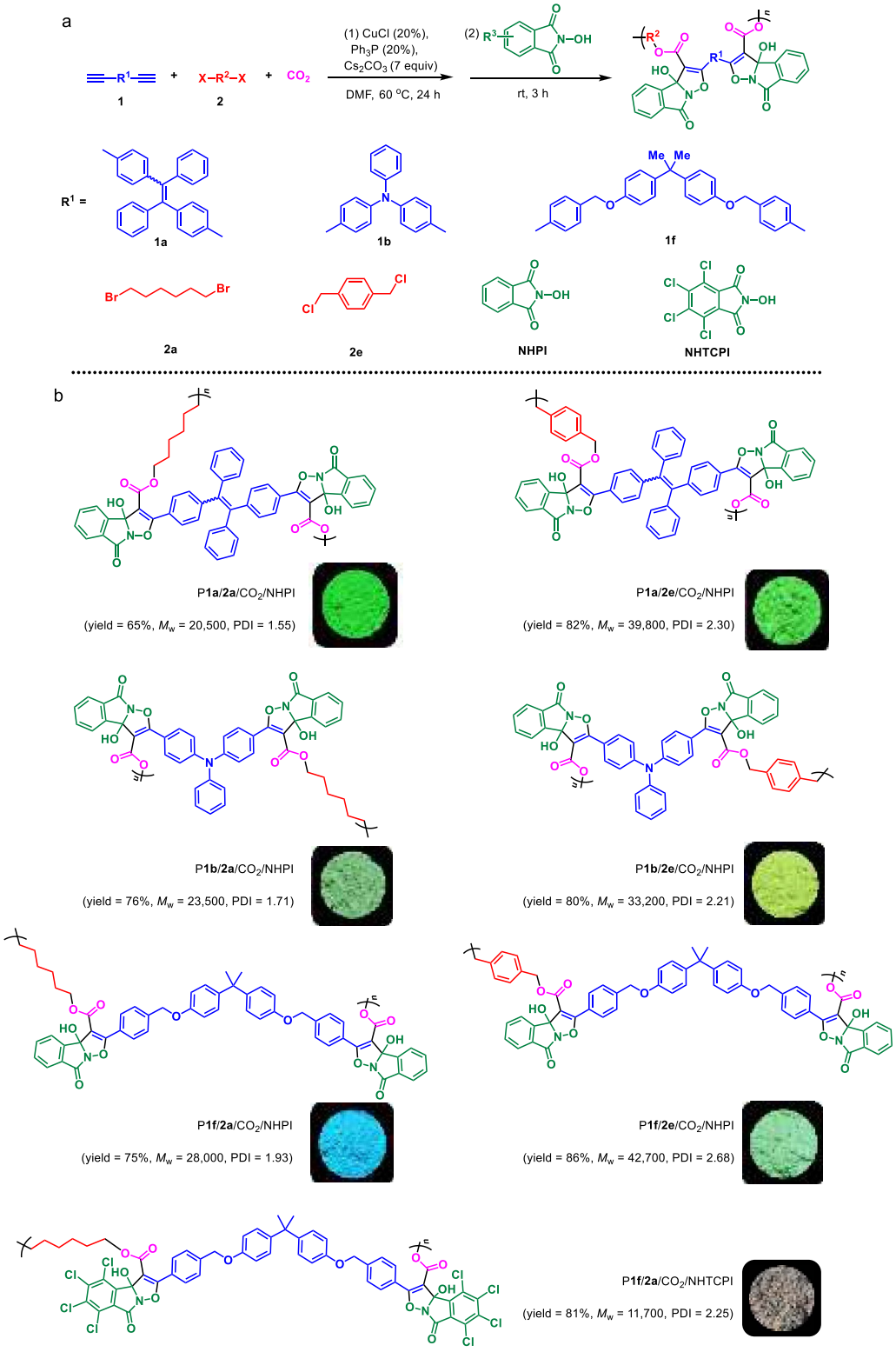

Figure 5. (a) FCTPs of diynes, dihalides, CO_2, and NHPI. (b) Chemical structures, yields, M_ws, PDIs, and their corresponding solid-state fluorescence images under a 365 nm UV lamp of polymers.

2.7. Silver ion detection

Inspired by the specific and sensitive detection of Fe^{3+} ions by poly(alkynoate)s, we hypothesized that the newly formed isoindolisoxazole rings of PHIIOs containing abundant O, N atoms and hydroxyl groups may have strong interactions with metal ions. **P1a/2a**/CO_2/NHPI containing TPE moieties also shows typical AIE feature (figures 6(a) and (b)), which show the highest fluorescent emission in 50% f_w of DMF/water mixture. Similar properties of **P1a/2e**/CO_2/NHPI

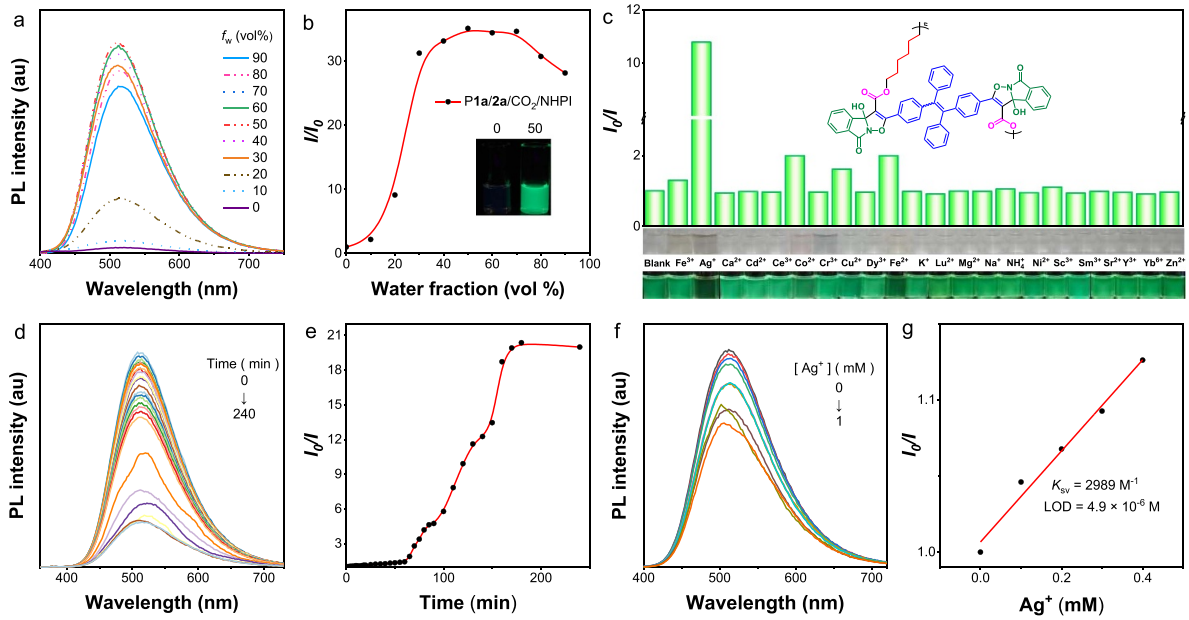

Figure 6. (a) PL spectra of P**1a/2a**/CO_2/NHPI in DMF/water mixtures with different f_ws. Concentration: 10 μM. λ_{ex}: 340 nm. (b) Plot of relative PL intensity versus water fraction in DMF/water mixtures, where I = peak intensity in DMF/water mixtures and I_0 = peak intensity in pure DMF. Inset: photographs of P**1a/2a**/CO_2/NHPI in pure DMF and DMF/water mixture with 50% water. (c) Relative PL intensity (I_0/I) of P**1a/2a**/CO_2/NHPI in DMF/water mixtures with f_w of 50% versus different metal ions after interaction for 120 min (polymer concentration of 10 μM, metal ion concentration of 6 mM. λ_{ex}: 340 nm). Inset: corresponding photographs of P**1a/2a**/CO_2/NHPI probes interacting with different metal ions taken under daylight and UV light at 365 nm, respectively. (d) PL spectra of P**1a/2a**/CO_2/NHPI interacting with Ag^+ ions at ten-minute intervals over 240 min. (e) Stern-Volmer plots of I/I_0 of P**1a/2a**/CO_2/NHPI versus time, where I = peak intensity and I_0 = peak intensity at 0 min. (f) PL spectra of P**1a/2a**/CO_2/NHPI in response to Ag^+ at different concentrations. (g) Linear relationship between I/I_0 and Ag^+ concentration at 512 nm, where I and I_0 are the fluorescence intensities of silver ions with different [Ag^+] and that without Ag^+, respectively.

were observed (figures S93-S94). Under the same conditions, 22 metal cations were mixed with the nanoaggregates of P**1a/2a**/CO_2/NHPI. We were surprised to find that there was no obvious fluorescence change in the 22 ions including Fe^{3+} ions. But after observation for 2 h, the Ag^+ ions gradually darkened the color of the probe solution in daylight and weakened the fluorescence of the probe under ultraviolet lamp (figure 6(c)). The response curve of Ag^+ ions to polymer fluorescence with time (figure 6(d)) showed that the fluorescence intensity of the polymer tended to stabilize after about 180 min (figure 6(e)). In addition, to study the sensitivity of the polymer to the quenching response of Ag^+ ions, titration experiments of silver ions on P**1a/2a**/CO_2/NHPI were carried out. The fluorescence curves were recorded after 180 min of interaction between the polymer probe and different concentrations of Ag^+ ions, and the Stern–Volmer curve of relative PL intensity (I_0/I) versus [Ag^+] shows a good linear relationship. The quenching constant and LOD were calculated to be 2989 M^{-1} and 4.90 $\times$ 10^{-6} M, respectively.

The quenching mechanism of P**1a/2a**/CO_2/NHPI for Ag^+ selective detection may be that electrons from the reducing functional groups (−OH) [43] of the polymer transfer to silver ions by electrostatic interaction/complexation, and then chemical reactions occur to reduce the silver ions to elemental silver. The resulting silver nanoparticles darken the color of the polymer probe solution, absorb the excitation light and the fluorescence emitted by the polymer, and then quench the fluorescent probe. Dynamic light scattering tests were carried out on polymer solutions before and after the addition of silver ions. As shown in (figure S95), the particle size of the probe before the addition of silver ions was 231 nm, but after adding Ag^+ ions for 3 h, the particle size of the mixture increased significantly to 1544 nm, implying strong interaction between the probe and the Ag^+ ions. X-ray photoelectron spectroscopy (XPS) and Auger electron spectroscopy (AES) further proved our conjecture. After interaction with P**1a/2a**/CO_2/NHPI, the $3d_{5/2}$ peak of $AgNO_3$ was changed from 368.26 eV to 368.34 eV (figures S96(a) and (b), and the Auger transition energy was changed from 355.9 eV to 356.5 eV (figures S96(c) and (d)), respectively. The new peaks were consistent with the standard XPS and AES peak positions of the element silver [44]. The results proved that the Ag^+ ions were reduced to the element silver by the polymer.

2.8. Plausible polymerization mechanism

According to our previous work and literature [26, 32, 45], the probable mechanism of this FCTP was proposed in scheme 3. There are probably seven main steps in the polymerization process: copper acetylide generation, CO_2 insertion, propiolic acid ester formation, zwitterion generation, Michael addition, cyclization, and rearrangement. The detailed processes are listed as follows. (a) Under the action of the base Cs_2CO_3 and the ligand Ph_3P, the terminal alkynes are easily deprotonated

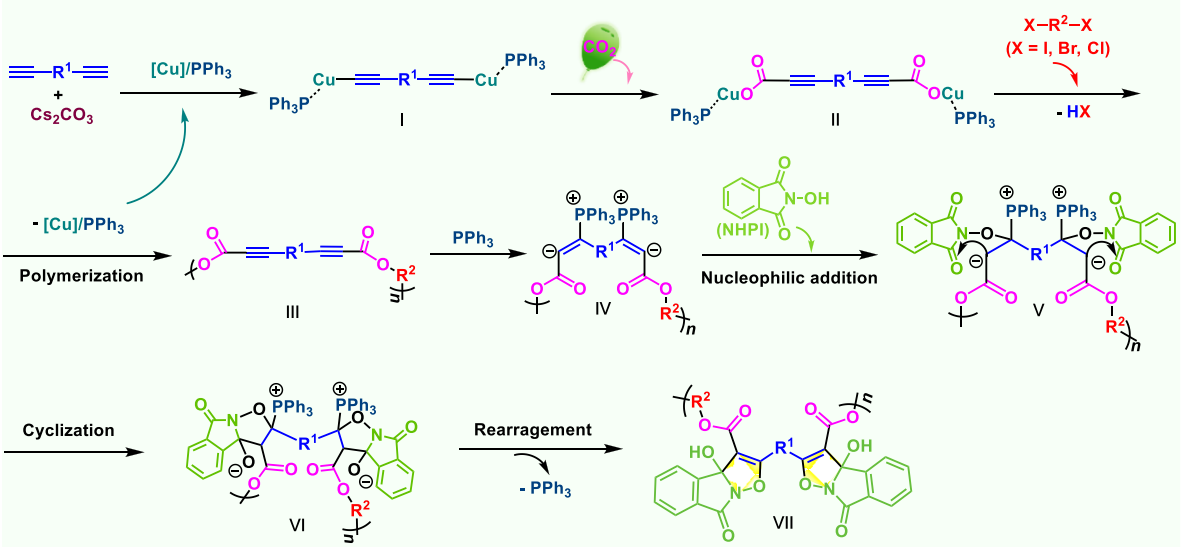

Scheme 3. The probable mechanism of the FCTP.

to form the intermediate copper acetylides (I) with CuCl. (b) Next, CO_2 molecules are inserted into the copper acetylides to form copper alkynates (II). (c) II is then polymerized with alkyl dihalides to form poly(alkynoate)s (III) via a step-growth polymerization. (d) Afterwards, the electron-deficient alkyne groups coordinate with the electron-rich Ph_3P to form zwitterions IV. (e) NHPI and IV undergo a Michael addition to yield V. (f) V is converted into VI by intramolecular nucleophilic addition and cyclization. (g) Finally, stable ring-fused PHIIOs are produced by leaving Ph_3P and rearrangement.

3. Conclusion

In summary, we have successfully realized an efficient CuCl/PPh_3-catalyzed MCP of terminal alkynes, dihalides, and CO_2 under mild conditions (rt—60 °C, atmospheric pressure), and a library of functional poly(alkynoate)s with high molecular weights were obtained. Meanwhile, high reactivity and excellent monomer universality allow for a wider extension of the monomers to be used in this polymerization, such as dihalides with different halogens (Cl, Br, I), alkyl and aryl diynes. In addition, the successful introduction of TPE groups endows poly(alkynoate)s with AIE characteristics, which could be used as fluorescence probe to instantaneously, specifically, and sensitively detect Fe (III) ions with a low LOD of 1.79×10^{-7} M. Notably, with abundant activated alkynyls in the main chain, poly(alkynoate)s can be post-modified *in situ* via a 'one-pot, two-step, four-component' tandem polymerization to yield PHIIOs, and the grafting ratio is up to 100%. Moreover, the AIE PHIIO can specifically detect Ag(I) ion with a low LOD of 4.90×10^{-6} M. Therefore, this work not only provides a low-energy strategy for the chemical fixation of CO_2 with low-cost catalysts, but also established efficiently CO_2-based MCP and multicomponent tandem polymerization to prepare multifunctional polymers with high molecular weight in high yield.

4. Future perspectives

The future of CO_2-based MCP under ambient conditions holds significant promise for sustainable polymer synthesis and carbon utilization. Key advancements will likely focus on catalytic innovation, with organocatalysts and enzyme-mimetic systems enabling energy-efficient CO_2 incorporation into high-value polymers such as polycarbonates and non-isocyanate polyurethanes. Concurrently, emerging research directions, including dynamic covalent chemistry for self-healing materials and AI-assisted catalyst design, could further optimize monomer selectivity and polymer performance. To bridge the gap between laboratory research and industrial adoption, scalable processes like solvent-free and continuous-flow polymerization will be critical. Moreover, integrating MCP with carbon capture technologies may transform CO_2 emissions into functional polymers for applications ranging from packaging to biomedicine. Despite these opportunities, challenges persist, particularly in overcoming CO_2's inherent thermodynamic stability and achieving cost-competitive production. However, with supportive policy frameworks and rigorous lifecycle assessments, CO_2-based MCP could emerge as a cornerstone of circular carbon economies. By uniting advances in green chemistry, materials science, and process engineering, this approach offers a transformative pathway toward sustainable manufacturing.

Acknowledgment

Funding This work was financially supported by the National Natural Science Foundation of China (nos. 22479102, 22001078), the Guangdong Talent Program (no. 2023TQ07L822), the Guangdong Basic and Applied Basic Research Foundation (no. 2024A1515011716), and the startup funding of Songshan Lake Materials Laboratory (no. Y1D1031H311).

Conflict of interest

The authors declare no competing interest.

Authors contribution

Tingzhu Duan: Data acquisition, Formal analysis, Writing—original draft, review & editing. Tianbai Xiong: Formal analysis. Lei Li: Formal analysis. Jia Wang: Conceptualization, Formal analysis, Supervision, Funding acquisition, Writing—original draft, review & editing. Xin Wang: Supervision, Funding acquisition, Writing—review & editing.

ORCID iD

Jia Wang 0000-0001-5851-3579

References

[1] Fuentes Andrade B, Buchwitz M, Reuter M, Bovensmann H, Richter A, Boesch H and Burrows J P 2024 A method for estimating localized CO_2 emissions from co-located satellite XCO_2 and NO_2 images *Atmos. Meas. Tech.* **17** 1145–73

[2] Mercer J H 1978 West Antarctic ice sheet and CO_2 greenhouse effect: a threat of disaster *Nature* **271** 321–5

[3] Qiu L-Q, Li H-R and He L-N 2023 Incorporating catalytic units into nanomaterials: rational design of multipurpose catalysts for CO_2 valorization *Acc. Chem. Res.* **56** 2225–40

[4] Song Q-W, Zhou Z-H and He L-N 2017 Efficient, selective and sustainable catalysis of carbon dioxide *Green Chem.* **19** 3707–28

[5] Yang G-W, Zhang Y-Y, Xie R and Wu G-P 2020 Scalable bifunctional organoboron catalysts for copolymerization of CO_2 and epoxides with unprecedented efficiency *J. Am. Chem. Soc.* **142** 12245–55

[6] Yang G-W, Xu C-K, Xie R, Zhang Y-Y, Zhu X-F and Wu G-P 2021 Pinwheel-shaped tetranuclear organoboron catalysts for perfectly alternating copolymerization of CO_2 and epichlorohydrin *J. Am. Chem. Soc.* **143** 3455–65

[7] Reiter M, Kronast A, Kissling S and Rieger B 2016 In situ generated ABA block copolymers from CO_2, cyclohexene oxide, and poly(dimethylsiloxane)s *ACS Macro Lett.* **5** 419–23

[8] Yu Y, Gao B, Liu Y and Lu X-B 2022 Efficient and selective chemical recycling of CO_2-based alicyclic polycarbonates via catalytic pyrolysis *Angew. Chem., Int. Ed.* **61** e202204492

[9] Huang Y, Xu L, Hu R and Tang B Z 2020 Cu(I)-catalyzed heterogeneous multicomponent polymerizations of alkynes, sulfonyl azides, and NH_4Cl *Macromolecules* **53** 10366–74

[10] Geiselhart C M, Mutlu H and Barner-Kowollik C 2021 Passerini multicomponent reactions enabling self-reporting photosensitive tetrazole polymers *ACS Macro Lett.* **10** 1159–66

[11] Chen L, Hu R and Tang B Z 2025 Facile synthesis of functional polytrithiocarbonates from multicomponent tandem polymerizations of CS_2, thiols, and alkyl halides *J. Am. Chem. Soc.* **147** 1134–46

[12] Zhu G, Lin N, Wu X, Shi J, Tong B, Cai Z, Zhi J and Dong Y 2022 Multicomponent spiropolymerization of diisocyanides, activated alkynes, and bis-anhydrides *Macromolecules* **55** 6150–9

[13] Tuten B T, De Keer L, Wiedbrauk S, Van Steenberge P H M, D'Hooge D R and Barner-Kowollik C 2019 Visible-light-induced passerini multicomponent polymerization *Angew. Chem., Int. Ed.* **58** 5672–6

[14] Xu L, Zhou T, Liao M, Hu R and Tang B Z 2019 Multicomponent polymerizations of alkynes, sulfonyl azides, and 2-Hydroxybenzonitrile/2-Aminobenzonitrile toward multifunctional iminocoumarin/quinoline-containing poly(N-sulfonylimine)s *ACS Macro Lett.* **8** 101–6

[15] Huang Y, Hu R and Tang B Z 2024 Multicomponent polymerization of sulfur, diynes, and aromatic diamines and facile tuning of polymer backbone structures *Macromolecules* **57** 6568–76

[16] He B, Zhang J, Zhang H, Liu Z, Zou H, Hu R, Qin A, Kwok R T K, Lam J W Y and Tang B Z 2020 Catalyst-free multicomponent tandem polymerizations of alkyne and amines toward nontraditional intrinsic luminescent poly(aminomaleimide)s *Macromolecules* **53** 3756–64

[17] Wang Y, Zhu L, Chen W, Zhou Z, Zhang Z and Hadjichristidis N 2022 Bimetallic Cu(I)/Rh(II) relay catalysis for multicomponent polymerization through carbene intermediates *Macromolecules* **55** 643–51

[18] Wang X, Liu C, Xing Z, Suo H, Qu R, Li Q and Qin Y 2022 Furfural-based polyamides with tunable fluorescence properties via Ugi multicomponent polymerization *Macromolecules* **55** 8857–65

[19] Cao W, Dai F, Hu R and Tang B Z 2020 Economic sulfur conversion to functional polythioamides through catalyst-free multicomponent polymerizations of sulfur, acids, and amines *J. Am. Chem. Soc.* **142** 978–86

[20] Chen K, Cui C, Li Z, Song Z, Zhang Q, Wu Y, Ge Z, Cheng Y and Zhang Y 2023 Thioaminal covalent adaptable networks via thiol–aldehyde–amine multicomponent polymerization *ACS Macro Lett.* **12** 543–8

[21] Chen F, Fan D, Wang D, Han T and Tang B Z 2024 One-pot four-component synthesis of acid-responsive and degradable heterochain polymers with nonconventional luminescence *Macromolecules* **57** 4993–5006

[22] Han T *et al* 2018 Facile multicomponent polymerizations toward unconventional luminescent polymers with readily openable small heterocycles *J. Am. Chem. Soc.* **140** 5588–98

[23] Wu X, He J, Hu R and Tang B Z 2021 Room-temperature metal-free multicomponent polymerizations of elemental selenium toward stable alicyclic poly(oxaselenolane)s with high refractive index *J. Am. Chem. Soc.* **143** 15723–31

[24] He J, Zheng N, Xie D, Zheng Y and Song W 2020 Multicomponent polymerization toward biodegradable polymers with diverse responsiveness in tumor microenvironments *Polym. Chem.* **11** 1198–210

[25] Song B, Qin A and Tang B Z 2022 Syntheses, properties, and applications of CO_2-based functional polymers *Cell Rep. Phys. Sci.* **3** 100719

[26] Liu D, Song B, Wang J, Li B, Wang B, Li M, Qin A and Tang B Z 2021 CO_2-involved and isocyanide-based three-component polymerization toward functional heterocyclic polymers with self-assembly and sensing properties *Macromolecules* **54** 4112–9

[27] Fu W, Dong L, Shi J, Tong B, Cai Z, Zhi J and Dong Y 2018 Multicomponent spiropolymerization of diisocyanides, alkynes and carbon dioxide for constructing 1,6-Dioxospiro[4,4]Nonane-3,8-Diene as structural units under one-pot catalyst-free conditions *Polym. Chem.* **9** 5543–50

[28] Song B, Bai T, Xu X, Chen X, Liu D, Guo J, Qin A, Ling J and Tang B Z 2019 Multifunctional linear and hyperbranched five-membered cyclic carbonate-based polymers directly

generated from CO_2 and alkyne-based three-component polymerization *Macromolecules* **52** 5546–54
[29] Oi S, Fukue Y, Nemoto K and Inoue Y 1996 Synthesis of poly(alkyl alkynoates) from diynes, CO_2, and alkyl dihalides by a copper(I) salt catalyst *Macromolecules* **29** 2694–5
[30] Song B, He B, Qin A and Tang B Z 2017 Direct polymerization of carbon dioxide, diynes, and alkyl dihalides under mild reaction conditions *Macromolecules* **51** 42–48
[31] Song B, Zhang R, Hu R, Chen X, Liu D, Guo J, Xu X, Qin A and Tang B Z 2020 Site-selective, multistep functionalizations of CO_2-based hyperbranched poly(alkynoate)s toward functional polymetric materials *Adv. Sci.* **7** 2000465
[32] Xie J-N, Yu B, Guo C-X and He L-N 2015 Copper(I)/phosphine-catalyzed tandem carboxylation/annulation of terminal alkynes with ambient pressure of CO_2: one-pot access to 3a-Hydroxyisoxazolo [3,2-a]Isoindol-8(3aH)-Ones *Green Chem.* **17** 4061–7
[33] Wang J, Li B, Xin D, Hu R, Zhao Z, Qin A and Tang B Z 2017 Superbase catalyzed regio-selective polyhydroalkoxylation of alkynes: a facile route towards functional poly(vinyl ether)s *Polym. Chem.* **8** 2713–22
[34] Li B, Feng B, Wang J and Qin Y 2024 Recent progress on polymerization-induced emission *Luminescence* **39** e4630
[35] Jing Y-N, Li S-S, Su M, Bao H and Wan W-M 2019 Barbier hyperbranching polymerization-induced emission toward facile fabrication of white light-emitting diode and light-harvesting film *J. Am. Chem. Soc.* **141** 16839–48
[36] Zhang H *et al* 2020 Clusterization-triggered emission: uncommon luminescence from common materials *Mater. Today* **32** 275–92
[37] Xiong H, Ramkumar N, Chiou M-F, Jian W, Li Y, Su J-H, Zhang X and Bao H 2019 Iron-catalyzed carboazidation of alkenes and alkynes *Nat. Commun.* **10** 122
[38] Kim H and Koo B 2021 Iron(III) sensors based on the fluorescence quenching of poly(phenylene ethynylene)s and iron-detecting PDMS pads *Macromol. Res.* **29** 360–4
[39] Huang W, Yan H, Niu S, Du Y and Yuan L 2017 Unprecedented strong blue photoluminescence from hyperbranched polycarbonate: from its fluorescence mechanism to applications *J. Polym. Sci. A* **55** 3690–6
[40] Wang J, Li M, Xu L, Huang D, Qin A and Wang X 2024 Ethynyl-directed dual $C(sp^3)$–H activation polymerization to construct regio- and stereoregular $C(sp^3)$–$C(sp^3)$ bond polymers *Macromolecules* **57** 122–31
[41] Wang J, Tian T, Zhang R, Li M, Chen J, Qin A and Tang B Z 2024 Efficient conversion of inert nitriles to multifunctional poly(5-amino-1,2,3-triazole)s via regioselective click polymerization with azide monomers under ambient conditions *J. Am. Chem. Soc.* **146** 6652–64
[42] Pandová I, Rimár M, Panda A, Valíček J, Kušnerová M and Harničárová M 2020 A study of using natural sorbent to reduce iron cations from aqueous solutions *Int. J. Environ. Res. Public Health* **17** 3686
[43] Peng H, Guo H, Gao P, Zhou Y, Pan B and Xing B 2021 Reduction of silver ions to silver nanoparticles by biomass and biochar: mechanisms and critical factors *Sci. Total Environ.* **779** 146326
[44] Kaushik V K 1991 XPS core level spectra and auger parameters for some silver compounds *J. Electron Spectrosc. Relat. Phenom.* **56** 273–7
[45] Liu D, Zhang H, Zhang L, Wang J, Chang Z and Cong H 2024 CS_2-based one-pot multicomponent tandem polymerization toward functional polybenzothiazoles *Polym. Chem.* **15** 2408–15